SITE SPECIFIC NON-LINEAR GROUND RESPONSE ANALYSIS AND SOIL STRUCTURE INTERACTION STUDY OF NEWLY CONSTRUCTED DHARAHARA TOWER

Santosh Katuwal[1] * **, Subeg Man Bijukchhen**[2]**, Chandra Kiran Kawan**[3]**, Anjali Shilpakar**[4]

[1]Department of Civil Engineering, Kantipur City College, Purbanchal University
[2] Research and Development Unit, Khwopa Engineering College, Purbanchal University
[3] Research and Development Unit, Khwopa College of Engineering, Tribhuvan University
[4] Department of Roads, Government of Nepal

Abstract

This study investigates the seismic performance of the recently reconstructed Dharahara tower, a historically significant monument in Nepal, that has experienced damage in past earthquakes and was completely destroyed in the recent Gorkha earthquake. Ground Response Analysis (GRA) and Soil-Structure Interaction (SSI) investigations are conducted to assess its structural behavior. GRA includes free field and structure-influenced analyses, with subsequent comparative assessment. Additionally, 3D non-linear finite element analysis is employed to derive equivalent spring constants representing soil and foundation characteristics, which are incorporated into the SSI analysis. These computed spring constants are used to model support conditions, allowing for an evaluation of the super-structural response. The study also employs non-linear dynamic analysis to compare structural responses between fix-based and spring-based models. The results indicate that the presence of the structure significantly influences surface wave motion amplification in GRA, resulting in peak ground accelerations (PGAs) that exhibit de-amplification in the free field and amplification in the presence of the structure. Furthermore, the introduction of an equivalent spring system in the soil-structure model changes the system's vibration period and damping characteristics, leading to enhanced dynamic response compared to the fixed-base model.

Keywords: Ground response analysis, Soil structure interaction, HS small soil model, Plastic analysis, Interface element, Spring-based support

1. Introduction

Nepal, located in the seismically active Himalayan region, faces recurrent and devastating earthquakes. The 2015 Gorkha earthquake (7.8Mw) serves as a stark example, causing 8,970 fatalities, injuring 22,303 people, and damaging 6,266 public buildings, 798,897 private residences, and cultural heritage sites, including the historic Dharahara tower (Subedi and Chhetri, 2019). Originally built in 1832, the tower underwent significant damage during the 1834 earthquake but survived. However, the 1934 Nepal-Bihar earthquake led to its complete destruction, with only a few stories remaining intact. Prime Minister Juddha Samser Janga Bahadur Rana oversaw its reconstruction, which endured until the 2015 Gorkha Earthquake (Udhyami, 2017). The current Dharahara tower in Sundhara, Kathmandu, is situated at latitude: $27^o42'1.88$" and longitude: $85^o18'43.03$", at the center of the Kathmandu valley, characterized by tectonic forces from the Indian and Eurasian plates. These forces altered the geological history, leaving thick, unconsolidated lacustrine deposits that amplify seismic activity by affecting wave parameters (Bijukchhen et al., 2017).

Most structures in the Kathmandu valley, including Dharahara, were designed without accounting for soil-structure interaction, assuming fixed-base support. This ar-

*Corresponding author: Santosh Katuwal
Department of Civil Engineering, Kantipur City College
Email: er.santoshkatuwal@gmail.com
(Received: Nov. 22, 2022, Accepted: Sept. 30, 2023)
https://doi.org/10.3126/jsce.v10i1.61014

ticle explores the profound influence of surface wave motion on structural dynamics, highlighting its impact on wave motion amplification and de-amplification, particularly in the presence of buildings. The research aims to shed light on the significant variations in ground motion amplification caused by soil-structure interaction and nonlinear soil behavior. By employing an equivalent spring system to model this interaction, the study reveals a notable increase in vibration period and system damping compared to fixed-based models, emphasizing the importance of energy dissipation within the integrated soil-structure system.

2. Ground Response Analysis (GRA)

Assessing the seismic response at the surface of the Earth is a crucial aspect of designing structures to withstand earthquakes. 1D GRAs are a commonly employed method to evaluate how seismic waves change in amplitude as they travel from a deep seismic source through layers of soil and reach the surface. This approach is favored in engineering because it relies on a relatively straightforward site description and is computationally efficient. However, 1D SRAs oversimplify the three-dimensional nature of wave propagation by modeling horizontally polarized vertically propagating shear waves traveling upward through a one-dimensional soil column. This column represents a simplified scenario of soil layers that extend infinitely in the lateral directions. Due to this simplification, any differences between actual data and estimates derived from 1D SRA are not unexpected (Pretell et al., 2022, Kaklamanos et al., 2013, Afshari and Stewart, 2019, Baise et al., 2011, Stewart, 2008, Thompson et al., 2012).

Ground response analysis is vital in geotechnical earthquake engineering, aiming to predict surface wave motion through layered soil deposits. It comes in three dimensions: 1D, 2D, and 3D, chosen based on site conditions. Avoid 1D in sloping or irregular sites and complex soil conditions where neighboring structures affect each other. Typically, 2D suits retaining walls, earth dams, tunnels, while 3D addresses sites with variable soil properties in all dimensions. Complex subsurface geometry requires 2D or 3D analysis as 1D underestimates amplification patterns, especially for higher-frequency modes (Kramer, 1996, Riepl et al., 2000).

3. Soil Modeling and Soil Parameter Calculation

To assess ground response and plastic deformation behavior, we utilize the advanced "HS small" soil model, characterized by its hardening behavior and small strain stiffness, effectively capturing the soil's non-linear and irreversible characteristics. This model enables us to depict the response of the soil across a wide range of strain levels, spanning from very small strains to significant deformations.

3.1. Stiffness parameters

Table 1 presents the essential stiffness parameters required for modeling the HS small soil model, with a significant portion of these parameters obtainable through the assessment of the SPT-N value.

Where, E_{50}^{ref} is secant stiffness in standard drained triaxial text, E_{ur}^{ref} is unloading-reloading stiffness, m is power of stress-level dependency stiffness, N is SPT-N value, S_u=$0.5q_u$, and q_u is unconfined compressive strength of the soil in kN/m^2 can be calculated using correlation of SPT-N value $q_u = 11.491N$ (Abu-Hejleh et al., 2005).

3.2. Parameters describing variation of stiffness with strain

Initial or very small strain shear modulus, $(G_0) = \rho V_s^2$, the shear strain level $\gamma_{0.7}$ at which secant shear modulus is reduced to about 70% of G_0 (Skels and Bondars, 2017)(Equation 1).

$$\gamma_{0.7} = 10^{-4} + 5 * 10^{-6} * PI * (OCR)^{0.3} \quad (1)$$

In this study, soil is considered to be normally consolidated with an overconsolidation ratio (OCR) of 1, and the plasticity index is determined from field test data. The reference shear modulus at very small strains can be calculated as in Equation (2).

$$G_0^{ref} = 33 * \frac{2.97 - e^2}{1 + e} (N/mm^2) \quad (2)$$

3.3. Void ratio

In soil mechanics, the void ratio (e) represents the ratio of the volume of voids within a soil mass to the volume of its solid particles. A correlation between void ratio (e) and Standard Penetration Test (SPT) - N value for various soil types is used for the study. The correlation is expressed as $e = 1.202N^{-0.217}$ and yielded an R^2 value of 0.736 (Anbazhagan et al., 2017).

3.4. General failure parameters

In the context of soil failure analysis, several crucial parameters come into play, including cohesion (c), the internal angle of friction (ϕ), and the angle of dilatancy (ψ). Cohesion (c) represents the soil's shear strength component. The internal angle of friction, denoted as ϕ, characterizes the soil's ability to resist shear stresses and can be defined as $\phi = 0.3125N + 26.1261$, where N is a relevant parameter. Dilatancy pertains to the soil's property in which its volume increases under shear deformation. Once the internal angle of friction is determined, the soil's dilatancy angle (ψ) can

Table 1: Correlations for HS small soil model (Phien-Wej et al., 2012)

Soil Description	E_{50}^{ref} (kN/m^2)	m	E_{ur}^{ref} (kN/m^2)
Filling Ground	5000-7000	0.5	$5E_{50}^{ref}$
Soft and Medium Clay	$250S_u$	1	8 to $10E_{50}^{ref}$
Stiff Clay	$700N$	0.85	$10E_{50}^{ref}$
Clayey Sand & Silty/Sandy Clay	$900N$	0.85	$3E_{50}^{ref}$
Medium to Dense Sand	$750N$	0.8	$3E_{50}^{ref}$
Dense to Very Dense Sand	$1000N$	0.5	$3E_{50}^{ref}$
Hard Clay	$1100N$	0.8	$10E_{50}^{ref}$
Dark Grey Clay	$2500N$	0.8	$10E_{50}^{ref}$

be calculated using the correlation $\psi = \phi - 30$. The effective soil cohesion (c) is expressed in units of kilonewtons per square meter (kN/m^2) and is given by the following relations (Equation 3, 4)
For $1 < N \leq 25$;

$$c = 0.0464N + 0.0075 \tag{3}$$

For $25 < N < 52$;

$$c = 0.0702N - 0.5453 \tag{4}$$

3.5. Relationship between compression index and water content

In soil mechanics research, various equations have been formulated to establish a relationship between the compression index (C_c) and natural water content or degree of saturation (S). These equations often rely on the correlation coefficient (R^2) to assess their effectiveness. A noteworthy example, proposed by Azzouz et al. in 1976, offers a straightforward correlation between the compression index and natural water content (W_n in %), represented as $C_c = 0.01(W_n - 5)$ (Azzouz et al., 1976).

3.6. Shear wave velocity

Shear wave velocity constitutes a vital parameter in ground response analysis and significantly influences ground motion amplification calculations. Numerous methodologies exist for determining shear wave velocity within soil layers. Among the most widely acknowledged and utilized empirical formulas are those that rely on factors such as N-values derived from the Standard Penetration Test (SPT), soil layer depth, and geological epoch. In this research, we compute shear wave velocity through the correlation of SPT-N values, as presented in Table 2 (Dikmen, 2009).

3.7. Soil densities

Unit weight is a measure of the weight of a unit volume of the material. The bulk unit weight of the soil is computed

Table 2: Shear wave velocity from SPT -N value (Dikmen, 2009)

SN	Soil Type	V_s (m/s)
1	All Soil	58 $N^{0.39}$
2	Sand	73 $N^{0.33}$
3	Silt	60 $N^{0.36}$
4	Clay	44 $N^{0.48}$

as:

$$\text{Bulk unit weight}, \gamma(kN/m^3) = \frac{(G + S * e)\gamma_w}{(1 + e)}$$

Saturated unit weight (γ_{sat}) of soil can be computed directly from SPT -N value (Rahman, 2020):

$$\text{Saturated unit weight}, \gamma_{sat}(kN/m^3) = 16.8 + 0.15N$$

3.8. Damping parameters

Rayleigh damping, a composite damping mechanism encompassing both mass damping and stiffness damping components, is characterized by its representation as:

$$[C] = \alpha\,[M] + \beta\,[K]$$

Where, $[C]$ = Damping matrix of the system, $[M]$ = Mass matrix of the system, $[K]$ = Stiffness matrix of the system, and α & β = Rayleigh damping coefficients.

$$\xi = \frac{\beta\omega}{2} + \frac{\alpha}{2\omega} \tag{5}$$

The stiffness damping parameter exhibits linear behavior with a direct proportionality between the damping ratio (ξ) and the natural frequency (ω), while mass proportional damping demonstrates non-linear behavior due to its inverse relationship with ω (Equation 5). In Rayleigh damping, lower natural frequencies are primarily influenced by mass damping, and higher frequencies by stiffness damping. To calibrate damping coefficients α and β in PLAXIS

2D, it is essential to specify a target damping ratio ξ and related frequencies. It is recommended to maintain the same ξ value for both target-1 frequency (the natural frequency of the soil profile) and target-2 frequency, typically chosen between 0.5% and 2%. The fundamental frequency for target-1 under small strain conditions in a homogeneous soil deposit can be determined as:

$$f_1 = \frac{V_s}{4H}$$

Where, V_s represents shear wave velocity in m/s and H is layer thickness in m. The shear wave velocity V_s is computed using SPT -N value from Table 2. In this study, average shear wave velocity for each layer is computed and corresponding frequency is adopted as target-1 frequency. For the layered soil deposition, natural frequency of borehole log can be obtained as:

The total travel time through a layered soil deposit, denoted as t, is calculated as the summation of travel times through individual layers:

$$t = \sum_{i=1}^{n} \frac{H_i}{V_{si}}$$

The average shearwave velocity can be determined using relation $V_s = H/t$. Where, H is total depth of soil deposit. Therefore, fundamental frequency of soil deposit:

$$f_1 = \frac{V_s}{4H}$$

Furthermore, the estimation of target-2 frequency (f_2) is derived from target-1 frequency (f_1) through the relation:

$$f_2 = nf_1$$

Where, n is an odd integer which can be obtained from the

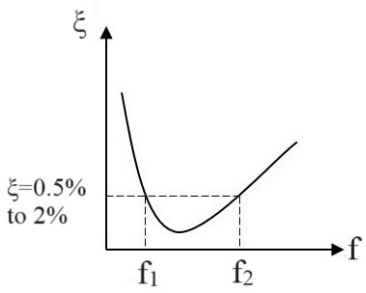

Figure 1: Relation between damping and frequencies

frequency ratio as:

$$\text{Ratio (N)} = \frac{\text{Fundamental frequency of input ground motion}}{\text{Frequency at target 1}}$$

Utilizing the parameter N enables the determination of n, whereby n represents the nearest odd integer greater than N. This selection is informed by the behavior of a shear beam, where the higher mode frequencies are odd multiples of the fundamental mode frequency of the beam, as described by Hudson (Hudson et al., 1994). The fundamental frequency of the input ground motion at the bedrock can be acquired through Fast Fourier Transform (FFT).

Example: If target-1 frequency is $1.2Hz$ and fundamental frequency of input ground motion is $3.2Hz$;

$$N = \frac{3.2}{1.2} = 2.67$$

$\therefore$ Odd number greater than N, (n) $= 3$

Now, target-2 frequency, $(f_2) = 3 * 1.2 = 3.6Hz$

3.9. Poisson's ratio

In the context of elastic material deformation, the Poisson ratio serves to quantify the correlation between transverse expansion and longitudinal contraction of a specimen. This ratio characterizes alterations in material shape while maintaining a constant volume (Marchenko et al., 2018). Table 3 provides approximate Poisson's ratio values utilized in the analysis of various soil types.

Table 3: Poisson's ratio for different soils (StructX, 2021)

Description	Poisson's Ratio (ν)
Sandy Clay	0.15-0.4
Dense Sand	0.2-0.4
Coarse Sand	0.15
Fine Sand	0.25
Silt	0.3-0.35
Clay	0.1-0.5
Saturated Clay	0.4-0.5
Unsaturated Clay	0.1-0.3

3.10. Properties of concrete

In the context of concrete modeling, the following material properties are considered: the unit weight of concrete (γ_c) is assumed to be 25 kN/m^3, the modulus of elasticity (E) is determined as $5000\sqrt{f_{ck}}$, (where f_{ck} signifies the characteristic strength of concrete in MPa), the Poisson's ratio (ν) is set at 0.2, and the shear modulus is determined using relation:

$$G = \frac{E}{2(1+\nu)}$$

3.11. Fundamental frequency of soil profile

In the context of a stratified soil deposit, the determination of the fundamental period and fundamental natural

frequency of the layered soil deposit hinges upon the utilization of the equivalent shear wave velocity, denoted as V_s. Consider a scenario where h_i represents the uniform thickness of the i^{th} layer, characterized by an average shear wave velocity denoted as V_{si}. In this context, the total travel time can be computed as:

$$t = \sum_{i=1}^{n} \frac{h_i}{V_{si}}$$

If H be the total depth of the soil profile, then equivalent shear wave velocity of the deposit consisting of n layers is $V_s = H/t$. Ultimately, fundamental frequency of the soil profile can be determined using relation, $f_o = V_s/4H$.

3.12. Example: Calculation of modeling parameters for HS small soil model

Identify the essential soil characteristics needed to define the 'HS Small' soil model when the Standard Penetration Test (SPT) N-value is 10, the water content is 25%, and the soil type is classified as stiff clay.

Solution:

From Table 1, stiffness related parameters can be computed as: $E_{50}^{ref} = 700N = 7000kN/m^2$, m=0.85, $E_{ur}^{ref} = 10E_{ur}^{ref} = 70000kN/m^2$

The void ratio; $e = 1.202N^{-0.217} = 0.7293$

Saturated unit weight; $\gamma_{sat} = 16.8+0.15N = 18.3kN/m^3$

Soil cohesion; $c = 0.0464N + 0.0075 = 0.4715kg/cm^2 = 46.23kN/m^2$

Internal angle of friction; $\phi = 0.3125N + 26.1261 = 29.251^o \approx 30^o$

Dilatancy angle; $\psi = \phi - 30 = 0$

Compression index; $C_c = 0.01(w_n - 5) = 0.01(25 - 5) = 20$

Plasticity index; $PI = (C_c/0.0259) - 1.88 = 5.84\%$

shear strain at which the shear modulus reduced to 70% of initial shear modulus, $\gamma_{0.7} = 10^{-4} + 5 * 10^{-6} * PI = 0.000129$

And $G_0^{ref} = 33 * \dfrac{2.97 - e^2}{1 + e} = 46.52MPa = 46.52 * 10^3 kN/m^2$

4. Soil Structure Interaction (SSI)

The response of a structure to earthquake shaking is influenced by interactions among three interconnected systems: the structure itself, its foundation, and the surrounding soil (Council, 2009). This phenomenon, known as Soil Structure Interaction (SSI) (Kramer, 1996), describes how soil response affects the structural response and vice versa. In structural engineering, structures are typically analyzed assuming fixed-base conditions, which may not fully capture their behavior, except for structures built on rock. These structures are characterized by mass (m), stiffness (k), and damping coefficient (c) representations. To facilitate the computation of SSI behavior, the phenomenon is divided into two main aspects: Kinematic Interaction, where the rigidity of a foundation relative to the soil constrains free field soil deformation, acting as a low-pass filter on shorter-wavelength ground motions, and resulting in rocking and twisting of the structure; and Inertial Interaction, which considers how the mass and pounding from the structure induce soil compliance, leading to additional soil deformation referred to as inertial interaction (Hoshiya and Ishii, 1983; Venture, 2012). The deformations due to kinematic interaction alone can be computed by assuming that the foundation has stiffness but no mass.

$$[M_{soil}]\{\ddot{u}_{KI}\} + [K^*]\{u_{KI}\} = -[M_{soil}]\{\ddot{u}_b(t)\} \quad (6)$$

This equation is solved for u_{KI}, which is referred as foundation input motion. Where $[M_{soil}]$ is the mass matrix assuming that the structure and foundation are massless.

The deformation due to inertial interaction can be computed using equation:

$$[M]\{\ddot{u}_{II}\} + [K^*]\{u_{II}\} = -[M_{str}]\{\ddot{u}_{KI}(t) + \ddot{u}_b(t)\}$$

Where, $[M_{str}]$ is the mass matrix assuming that soil is mass less.

4.1. Effect of building in free field ground motion

According to the study of Stewart, variations in spectral accelerations between foundation and free field conditions are linked to dimensionless parameters like embedment ratio, dimensionless frequency, and structure-to-soil stiffness ratio, influencing kinematic and inertial soil-structure interaction. Soil-structure interaction can amplify or de-amplify foundation-level motion across different frequencies due to both kinematic and inertial effects and localized soil nonlinearity beneath the foundation (Stewart, 2000). During an earthquake, the vibrating building alters ground motion by transmitting energy to the soil (Wong and Trifunac, 1975). Amplification depends on building type and layout (Ditommaso et al., 2007). Structures increase engineering ground motion parameters like PGA and spectral ordinates, with both experiments and simulations agreeing that structures modify earthquake-induced free field vibrations, rendering free field ground response analysis impractical in densely populated cities (Mucciarelli, 2009).

4.2. Interface element

In soil-structure interaction simulations using finite element modeling, the soil-structure interface is pivotal for realistic solutions. To prevent rigid connections between the structure and soil, interface elements must be defined. Without these, relative displacement and behaviors like slipping and gaping cannot be modeled (Sloot, 2019). Thin layer elements with suitable constitutive laws, correct thickness, and

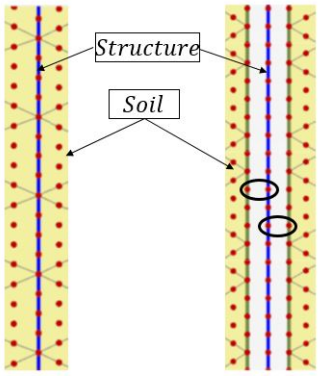

Figure 2: (a) Shared node between soil element and structure, (b) Node pair created by defining soil structure interface (Sloot, 2019)

deformation mode integration are used. In this study, we defined a thin layer interface element with a virtual thickness factor of 0.1 in PLAXIS 3D. This definition creates node pairs at the soil-structure interface, where each pair shares the same coordinates, as illustrated in Figure (2) (b).

Interface element between soil and structure are created as shown in Figure 3.

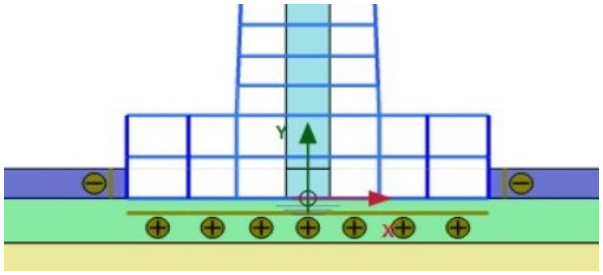

(a) 2D interface

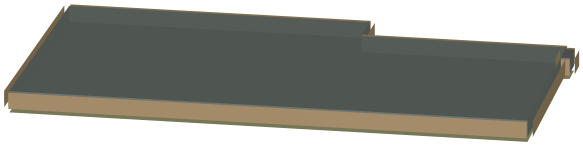

(b) 3D interface

Figure 3: Soil-structure interface element for 2D and 3D model

5. Methodology

The investigation is categorized into three main groups: 1) The Ground Response Analysis (GRA) utilizes surface wave motion, sourced either from 1D or 2D free field GRA, or from 2D GRA in the presence of a structure, as input for time history analysis. 2) Plastic deformation analysis involves conducting 3D soil-structure integrated plastic deformation analysis to determine spring stiffness at both ends of the columns for models with and without piles. 3) Dynamic analysis entails non-linear dynamic time history analysis to compare results between the spring-based model with and without pile foundations, as well as a fixed-based model.

5.1. Data collection

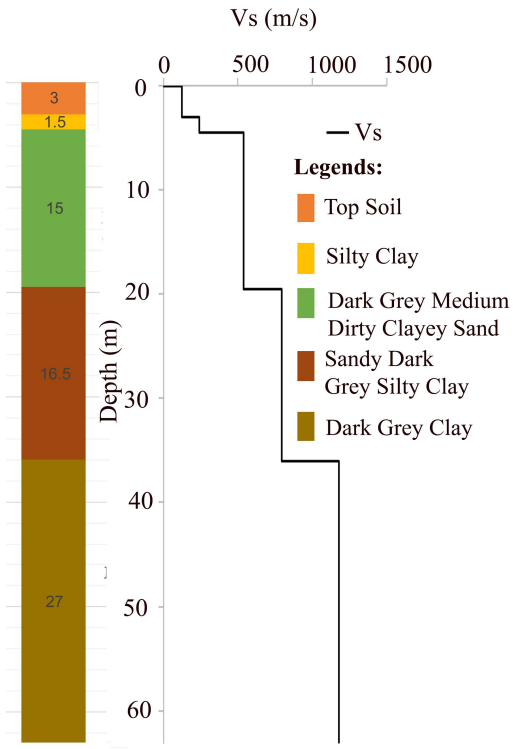

Figure 4: Borehole log and shear wave velocity profile of the Dharahara site

In data collection phase, structural, seismic and geotechnical data are collected from design and field test reports. Similarly, time history data is taken from the past recorded earthquake (Gorkha Earthquake, 2015) recorded at Kirtipur is taken for the analysis. For the study, 63m deep excavated borehole log is taken for the analysis which is shown in Figure 4. The lateral extent of the foundation is taken as 4W (W is the base width of the foundation) in both directions (Ghosh, 1971).

Outcropping earthquake motion recorded at Kirtipur station (Refer Figure 9) provided by the Faculty of Engineering at Hokkaido University (Takai et al., 2016) is used for the GRA and SSI study of the tower. The significant duration of the earthquake, calculated using the Arias intensity in percentage, falls between 5% and 95% of the Arias intensity as 38.22 seconds (Refer Figure 9).

5.2. Modeling for GRA

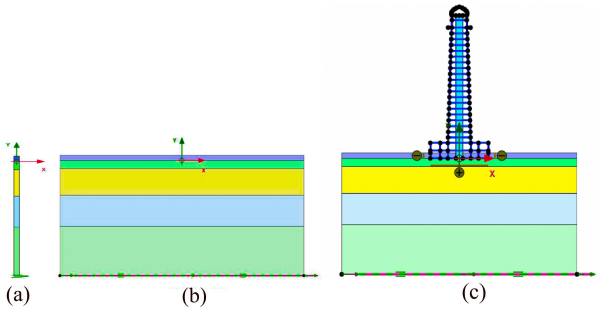

Figure 5: Model prepared for GRA (a) 1D free field (b) 2D free field (c) 2D with structure

The investigation of Ground Response Analysis (GRA) involves assessing essential parameters for soil and structural modeling (Section 3). These parameters are incorporated into both PLAXIS 2D and PLAXIS 3D. Geometrical soil modeling is based on borehole log data (Figure 4). For 1D GRA, a 1m x 63m borehole log is analyzed in PLAXIS 2D. Similarly, a 134m x 63m lateral soil area is modeled in PLAXIS 2D for 2D free field GRA and GRA in the presence of a structure (Figure 5) is modeled to perform GRA with the structural influence.

5.3. Soil structure integrated model

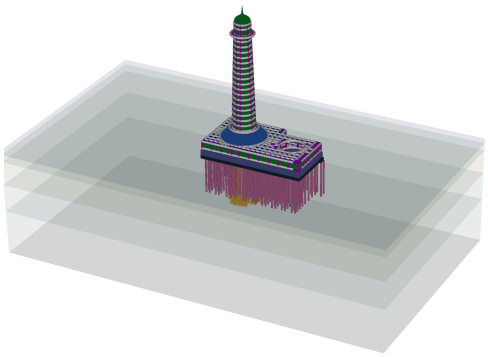

Figure 6: 3D soil-structure integrated model (with pile foundation)

3D soil-structural modeling (Figure 6) is performed using PLAXIS 3D to calculate spring coefficients through plastic deformation analysis. The model incorporates beam elements for beams and columns, plate elements for slabs, basements, and shear walls, and embedded beam elements for piles. Each pile, with a diameter of 700 mm, is located at two different depths: 21 meters with an end bearing capacity of 196.5 kN and 30 meters with an end bearing capacity of 228.5 kN (Seismo-Tech, 2018). These piles are modeled as shown in Figure 6. Spring coefficients are derived from reaction forces and deflection, both with and without pile foundation consideration. An interface element is introduced at the basement to prevent soil-structure tie.

5.4. Mesh generation

Analytical modeling is limited to regular and simple geometries, making it insufficient for real-world complexities. Hence, numerical modeling, specifically the Finite Element Method, is preferred. This approach discretizes the complex geometry into finite elements for individual calculations. The results are then combined to provide a comprehensive field solution. This study uses a 15-noded plane strain element for 1D and 2D GRA modeling, and a 10-noded tetrahedral element from PLAXIS 3D for three-dimensional soil-structure plastic deformation analysis. Generated mesh and deformed soil mass obtained from plastic deformation analysis is shown in Figure 7.

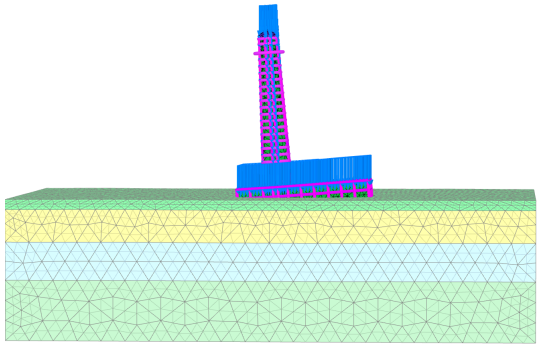

Figure 7: Generated mesh with deformed soil mass

5.5. Determination of spring stiffness representing soil

The spring constant is determined by creating a 3D soil and structure model with design loads in PLAXIS 3D, followed by conducting plastic analysis with and without considering the pile foundation. Reaction forces and deformations from this analysis are used to formulate a spring model depicted in Figure 14. Subsequently, spring constants are determined for each support based on the results of the plastic analysis in PLAXIS 3D.

$$\text{Spring coefficient along x-direction}(K_x) = \frac{Q_{13}}{u_x}$$

$$\text{Spring coefficient along y-direction}(K_y) = \frac{Q_{12}}{u_y}$$

$$\text{Spring coefficient along z-direction}(K_z) = \frac{N}{u_z}$$

Where, N is axial force, Q_{12} and Q_{13} are shear forces generated at connecting node of foundation and superstructure (refer Figure 8).

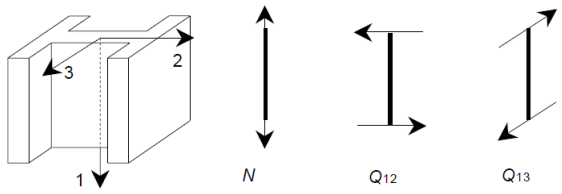

Figure 8: Axial and shear forces (Brinkgreve and Broere, 2006)

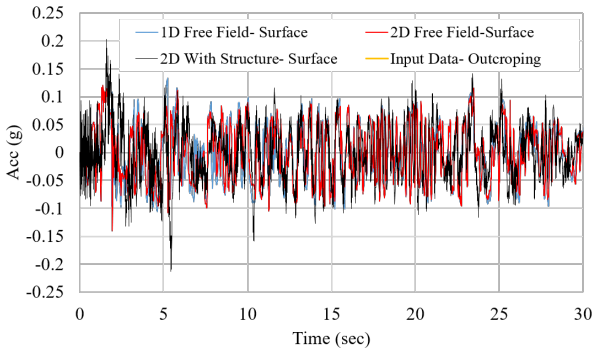

Figure 9: Comparison of generated surface wave motion

We incorporated the determined spring coefficients at the base of the columns as the support condition, as illustrated in Figure 14. Subsequently, we performed dynamic analysis on the superstructure using relevant time history data sourced from GRA.

6. Results and Discussions

6.1. Ground response analysis

The GRA utilizes the Gorkha Earthquake accelerogram recorded at the Kirtipur station, with a PGA value of 0.153g, approximated as outcropping bedrock motion. This recorded motion is applied at the base of a simulated soil layer, assuming the underlying soil deposition acts as engineering bedrock ($V_s > 750m/s$), as indicated by the shear wave velocity profile in Figure 4. The 1D GRA analysis in a free field condition resulted in a slightly lower PGA of 0.134g than the input PGA of 0.153g, while the 2D GRA analysis in a free field provided a PGA of 0.144g. The fundamental natural frequency of soil profile and fundamental predominant frequency of the wave motion are different; therefore, no resonance effect is observed while performing site response analysis; which resulted in slight deamplification of surface wave motion in free field vibration analysis. Notably, when considering the presence of a structure in the 2D GRA analysis, the PGA increased to 0.215g. Variation of ground motion amplification in the presence of structure is high due to kinematic and inertial effect of soil structure interaction as well as non-linear behavior of soil beneath the foundation.

The FFT is performed on time histories generated at the top of the soil for three different scenarios: 1D free field GRA, 2D free field GRA, and 2D GRA with structural influences. The results are depicted in Figure 10. The analysis revealed that the frequency ranges exhibit minimal variation in Fourier amplitude. The fundamental peaks of the FFT indicate consistent vibration frequencies at the top soil layer, with a predominant frequency of approximately 0.5Hz observed in all three scenarios: 1D free field GRA, 2D free field GRA, and 2D GRA with structural effects. This frequency coincides with significant spectral acceleration amplification at around 2 seconds, indicating a resonance effect (Refer Figure 10 and 11). This resonance has historically contributed to damage to the Dharahara tower during major earthquakes.

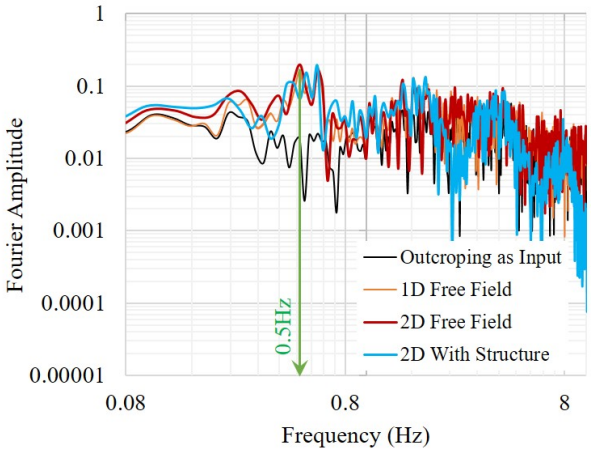

Figure 10: Comparison of Fourier amplitude spectra

The analysis reveals that PGA (Peak Ground Acceleration) in free field ground motion is slightly reduced in both 1D and 2D scenarios. However, when considering a tower structure in 2D ground response analysis, the PGA at the surface is amplified to some extent. This shows the significant role of the structure in amplifying ground motion compared to free field ground vibrations. Consequently, the surface wave motion generated by 2D ground response analysis, accounting for the structure, is chosen as the input time history for subsequent nonlinear dynamic analysis of superstructure.

Ground motion amplification in the presence of structures is influenced by various factors, including the

kinematic and inertial effects of soil-structure interaction and the nonlinear behavior of the foundation soil (Stewart, 2000). The structure's own vibration creates inertia, increasing the base shear and moment, leading to foundation sliding (due to inertial interaction) and rocking (due to kinematic interaction), ultimately resulting in ground motion amplification compared to free field ground vibration. The tall and heavy structure generates significant inertial forces and moments, promoting sliding and bending mechanisms, contributing to ground motion amplification. Additionally, the use of stiff shear wall mechanisms in the tower enhances kinematic interaction behavior (rocking and twisting), which, in turn, increases energy transfer to the foundation soil. The combination of reflected energy from both inertial and kinematic interactions has a substantial impact on wave motion amplification, with higher reflection leading to more extensive amplification.

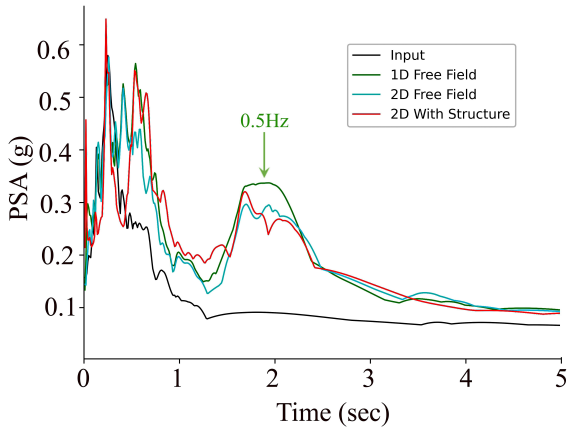

Figure 11: Comparison of response spectra obtained at the surface

6.2. Soil mass deformation

Figure 12 and Figure 13 illustrate the permanent deformation of soil, in which section planes A-A* and B-B* depict the deformation behavior induced by the superstructure. A-A* corresponds to the shorter direction of the soil model, while B-B* provides a clear view of the subsurface soil deformation pattern along the longer direction. Color gradients within the diagrams represent deformed values of the soil, with corresponding values displayed alongside each diagram. Figure 12 illustrates the observed dimensions of deformed soil without considering pile foundation: 65m along the shorter direction (Figure 12b), 86m along the longer direction (Figure 12c), a total depth of 30m, and a maximum vertical settlement of 120mm. Figure 13 depicts the soil deformation with a pile foundation, revealing a total deformed soil depth of 52m and a maximum vertical deflection of 48mm. The measurements indicate that the chosen soil dimensions are sufficient for the analysis. The results demonstrate that embedded piles distribute the superstructure load more widely in all directions, reducing soil settlement compared to sole basement foundations. This implies that pile foundations effectively control excessive soil settlement at the foundation level by transferring the load deeper into the soil.

6.3. Spring stiffness from soil settlement and reaction developed

The stiffness of the spring at the end of the columns are determined through plastic deformation analysis, considering both with and without pile foundations. This stiffness value is computed using the force generated by the superstructure load and the observed deformations at each end of the columns in all three directions, as detailed in Section 5.5. Subsequently, a spring-based model representing the underlying soil is created as illustrated in Figure 14.

Example calculation: The base reactions in the X, Y, and Z directions are as follows: $Q_{13} = 3.809kN$, $Q_{12} = 1.39kN$, and $N = 373.047kN$. Corresponding deflections are: $u_x = 0.003538m$, $u_y = 0.00053m$, and $u_z = 0.04375m$. Thus, the equivalent stiffness of the springs can be determined as:

$$K_x = \frac{Q_{13}}{u_x} = \frac{3.809}{0.003538} = 1076.488kN/m$$

$$K_y = \frac{Q_{12}}{u_y} = \frac{1.39}{0.00053} = 2629.092kN/m$$

$$K_z = \frac{N}{u_z} = \frac{373.047}{0.04375} = 8526.859kN/m$$

6.4. Structural response from THA

The studies indicate that considering the effect of the soil beneath has the effect of increasing the primary oscillation duration of the building, which is demonstrated in Table 4.

Table 4: Fundamental frequency and time period of the structure

Support condition	Fundamental Frequency (Hz)	Fundamental Period (Sec)
1. Fixed based	1.081	0.92539
2. Spring without pile foundation	1.011	0.98899
3. Spring considering pile foundation	1.006	0.99442

It is also observed that the consideration of soil-structure interaction leads to an increase in peak story displacement as compared to a fixed-based support condition. The visual

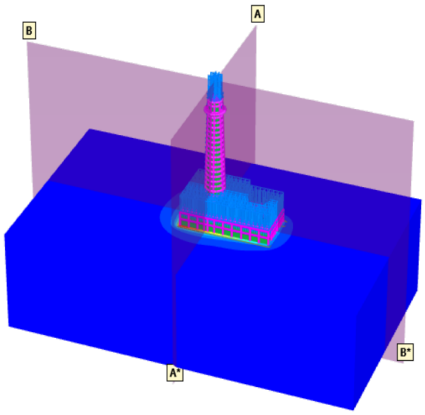

(a) Section planes

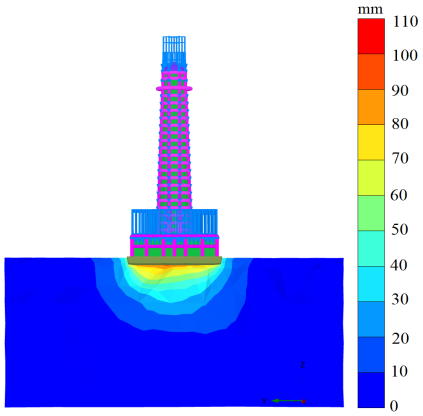

(b) Section A-A*

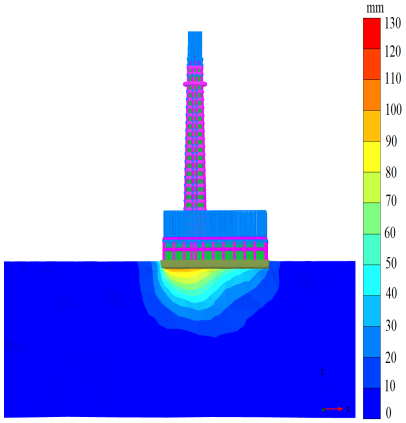

(c) Section B-B*

Figure 12: Soil deformation without pile foundation

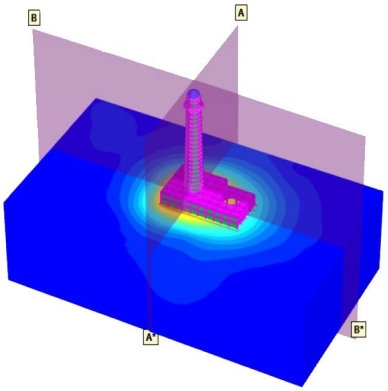

(a) Section planes

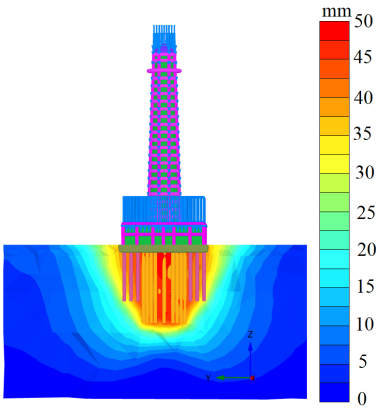

(b) Section A-A*

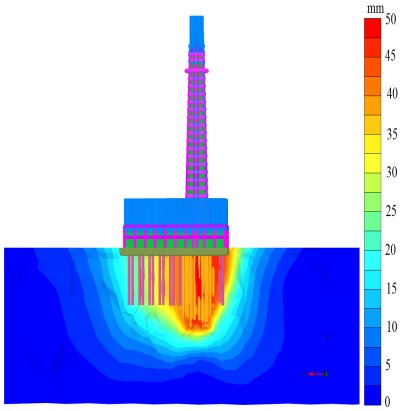

(c) Section B-B*

Figure 13: Soil deformation with pile foundation

representation in Figure 15(a) demonstrates that the spring-based model exhibits deformation initiation at the structure's base due to spring-based support, a phenomenon not observed in the fixed-based support scenario. This underscores the pivotal role of accounting for soil effects in structural analysis. Furthermore, the provision of lateral supports at the third floor in the spring-based model mitigates story deformation, thereby augmenting structural rigidity. According to IS 1893:2016, the structure's maximum allowable displacement is 277.6mm. Consequently, the obtained story displacement falls within the acceptable range. Figure 15(b) depicts a noteworthy reduction in peak floor

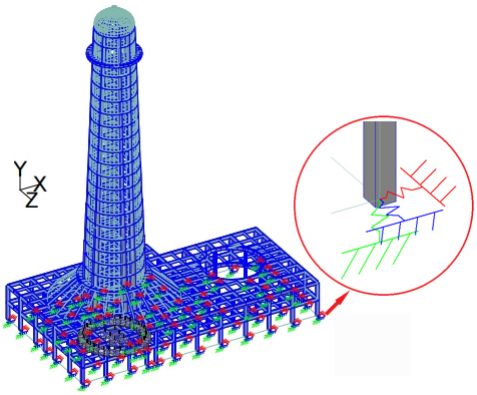

Figure 14: Spring model representing soil

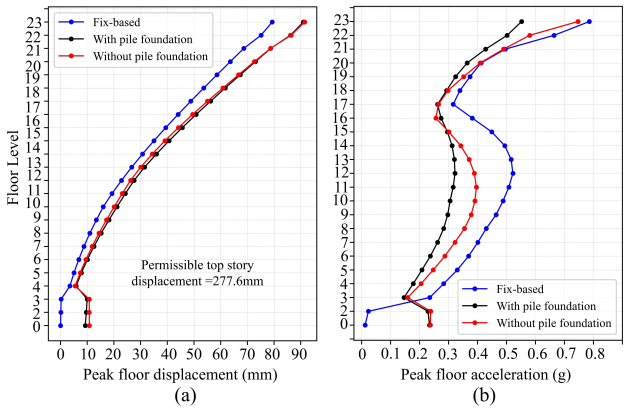

Figure 15: Structural response obtained from time history analysis

acceleration within the spring-based model, signifying a de-amplification of wave motion relative to the fixed-based model. This reduction is attributed to the dissipation of energy within the spring-based model. Additionally, modal vibration patterns influence peak floor acceleration values on upper stories, introducing fluctuations that delineate the impact of modal vibration throughout the tower height of tower.

7. Conclusion

In conclusion, research findings reveal that the fundamental natural frequency of the soil profile and the fundamental predominant frequency of wave motion exhibit a disparity, leading to the absence of resonance effects and resulting in a slight de-amplification of surface wave motion in free field site response analysis. Moreover, the analysis highlights the substantial influence of surface wave motion on wave motion amplification and de-amplification when structures are present. This phenomenon is attributed to energy transmission between the building and the soil, with variations in ground motion amplification primarily arising from the complex interplay of kinematic and inertial effects in soil-structure interaction and the non-linear behavior of the soil beneath foundations. Additionally, the study demonstrates that incorporating an equivalent spring system to represent the soil-structure model in dynamic analysis leads to increased vibration periods and system damping when compared to fixed-based models. This increase in damping can be attributed to the dissipation of energy within the soil-structure system, resulting in reduced elastic deformation of the structure.

References

Abu-Hejleh, N. M., O'Neill, M. W., Hanneman, D., & Attwooll, W. J. (2005). Improvement of the geotechnical axial design methodology for colorado's drilled shafts socketed in weak rocks. *Transportation research record*, *1936*(1), 100–107.

Afshari, K., & Stewart, J. P. (2019). Insights from california vertical arrays on the effectiveness of ground response analysis with alternative damping models. *Bulletin of the Seismological Society of America*, *109*(4), 1250–1264.

Anbazhagan, P., Uday, A., Moustafa, S. S., & Al-Arifi, N. S. (2017). Soil void ratio correlation with shear wave velocities and spt n values for indo-gangetic basin. *Journal of the Geological Society of India*, *89*(4), 398–406.

Azzouz, A. S., Krizek, R. J., & Corotis, R. B. (1976). Regression analysis of soil compressibility. *Soils and Foundations*, *16*(2), 19–29.

Baise, L., Thompson, E., Kaklamanos, J., & Dorfmann, L. (2011). Complex site response: Does one-dimensional site response work? *Proc. 4th IASPEI/IAEE International Symposium*.

Bijukchhen, S. M., Takai, N., Shigefuji, M., Ichiyanagi, M., Sasatani, T., & Sugimura, Y. (2017). Estimation of 1-d velocity models beneath strong-motion observation sites in the kathmandu valley using strong-motion records from moderate-sized earthquakes. *Earth, Planets and Space*, *69*(1), 1–16.

Brinkgreve, R., & Broere, W. (2006). Plaxis 3d foundation. reference manual. version 1.5.–delft. *Delft University of Technology*.

Council, B. S. S. (2009). Nehrp recommended seismic provisions for new buildings and other structures. *Rep. FEMA P*, *750*.

Dikmen, Ü. (2009). Statistical correlations of shear wave velocity and penetration resistance for soils. *Journal of Geophysics and Engineering*, *6*(1), 61–72.

Ditommaso, R., Gallipoli, M. R., Mucciarelli, M., & Ponzo, F. C. (2007). Effect of vibrating building on "free field" ground motion: From the bagnoli experiment to many-buildings simulation. *Proc. 4th Int. Conf. Earthq. Geot. Eng., CD-Rom edition, Paper*, (1388).

Ghosh, S. (1971). Dynamic stress analysis of axisymmetric structures under arbitrary loading.

Hoshiya, M., & Ishii, K. (1983). Evaluation of kinematic interaction of soil-foundation systems by a stochastic model. *International Journal of Soil Dynamics and Earthquake Engineering*, *2*(3), 128–134.

Hudson, M., Idriss, I., Beikae, M., et al. (1994). *Quad4m: A computer program to evaluate the seismic response of soil structures using finite element procedures and incorporating a compliant base*. Center for Geotechnical Modeling, Department of Civil; Environmental ...

Kaklamanos, J., Bradley, B. A., Thompson, E. M., & Baise, L. G. (2013). Critical parameters affecting bias and variability in site-response analyses using kik-net downhole array data. *Bulletin of the Seismological Society of America*, *103*(3), 1733–1749.

Kramer, S. L. (1996). *Geotechnical earthquake engineering*. Pearson Education India.

Marchenko, M., Mosicheva, I., & Aniskin, A. (2018). Estimation of poisson's ratio of soil using stiffness of loose soils. *Electronic Journal of the Faculty of Civil Engineering Osijek-e-GFOS*, *9*(16), 85–94.

Mucciarelli, M. (2009). Effect of buildings on free-field ground motion. In *Increasing seismic safety by combining engineering technologies and seismological data* (pp. 139–140). Springer.

Phien-Wej, N., Humza, M., & Aye, Z. Z. (2012). Numerical modeling of diaphragm wall behaviour in bangkok soil using hardening soil model. *Geotechnical Aspects of Underground Construction in Soft Ground–Viggiani (ed), Taylor & Francis Group, London*, 715–722.

Pretell, R., Ziotopoulou, K., & Abrahamson, N. A. (2022). Conducting 1d site response analyses to capture 2d vs spatial variability effects. *Earthquake Spectra*, *38*(3), 2235–2259.

Rahman, M. M. (2020, June). *Foundation design using standard penetration test (spt) n-value*. https://doi.org/10.13140/RG.2.2.23159.73123

Riepl, J., Zahradnik, J., Plicka, V., & Bard, P.-Y. (2000). About the efficiency of numerical 1-d and 2-d modelling of site effects in basin structures. *pure and applied geophysics*, *157*(3), 319–342.

Seismo-Tech. (2018, May). Final Report on Geotechnical Investigation at Dharahara, 2018.

Skels, P., & Bondars, K. (2017). Applicability of small strain stiffness parameters for pile settlement calculation. *Procedia Engineering*, *172*, 999–1006.

Sloot, M. V. D. (2019). Modelling soil-structure interaction: Interfaces [Accessed: 22-02-2021].

Stewart, J. P. (2000). Variations between foundation-level and free-field earthquake ground motions. *Earthquake Spectra*, *16*(2), 511–532.

Stewart, J. P. (2008). *Benchmarking of nonlinear geotechnical ground response analysis procedures*. Pacific Earthquake Engineering Research Center.

StructX. (2021). Poisson's ratio values for various soil types [Accessed: 08-02-2021].

Subedi, S., & Chhetri, M. B. P. (2019). Impacts of the 2015 gorkha earthquake: Lessons learnt from nepal. In *Earthquakes-impact, community vulnerability and resilience*. IntechOpen.

Takai, N., Shigefuji, M., Rajaure, S., Bijukchhen, S., Ichiyanagi, M., Dhital, M. R., & Sasatani, T. (2016). Strong ground motion in the kathmandu valley during the 2015 gorkha, nepal, earthquake. *Earth, Planets and Space*, *68*(1), 1–8.

Thompson, E. M., Baise, L. G., Tanaka, Y., & Kayen, R. E. (2012). A taxonomy of site response complexity. *Soil Dynamics and Earthquake Engineering*, *41*, 32–43.

Udhyami, B. (2017). Nepal in data back in time: Dharahara [Accessed: 28-03-2021].

Venture, N. C. J. (2012). Soil-structure interaction for building structures. *Nist Gcr*, 12–917.

Wong, H., & Trifunac, M. (1975). Two-dimensional, antiplane, building-soil-building interaction for two or more buildings and for incident planet sh waves. *Bulletin of the Seismological Society of America*, *65*(6), 1863–1885.